Zhu Feng (Orcid ID: 0000-0003-2409-151X)
Lai Xiaojing (Orcid ID: 0000-0003-4451-9421)
Chen Bin (Orcid ID: 0000-0001-8314-9991)

Kinetic control on the depth distribution of superdeep diamonds

Feng Zhu[1]*†, Jie Li[1]*, Jiachao Liu[1]‡, Xiaojing Lai[2,3], Bin Chen[2], and Yue Meng[4]

[1]Department of Earth and Environmental Sciences, University of Michigan, Ann Arbor, Michigan 48109, USA.

[2]Hawaii Institute of Geophysics and Planetology, University of Hawai'i at Mānoa, Honolulu, Hawai'i 96822, USA.

[3]Department of Geology and Geophysics, University of Hawai'i at Mānoa, Honolulu, Hawai'i 96822, U

[4]High Pressure Collaborative Access Team (HPCAT), X-Ray Science Division, Argonne National Lab, Argonne, Illinois 60439, USA.

*Corresponding author: Feng Zhu (fzhuum@umich.edu); Jie Li (jackieli@umich.edu)

†Current address:

Hawaii Institute of Geophysics and Planetology, University of Hawai'i at Mānoa, Honolulu, Hawai'i 96822, USA.

‡Current address:

Department of Geological Sciences, Jackson School of Geosciences, University of Texas at Austin, Austin, Texas, 78712, USA.

Key Points:

- Real-time tracking of diamond production from iron-magnesite reaction at high pressures and high temperatures

- Three-fold reduction in the rate of iron-magnesite reaction from 14.4 to 18.4 GPa

- Depth distribution of superdeep diamonds may be explained by reaction kinetics.

Abstract

Superdeep diamonds contain unique information from the sublithospheric regions of Earth's interior. Recent studies suggest that reaction between subducted carbonate and iron metal in the mantle plays an important role in the production of superdeep diamonds. It is unknown if this reaction is kinetically feasible in cold slabs subducted into the deep mantle. Here we present experimental data on real-time tracking of the magnesite-iron reaction at high pressures and high temperatures to demonstrate the production of diamond at the surface conditions of cold slabs in the transition zone and lower mantle. Our data reveal that the diamond production rate has a positive temperature dependence and a negative pressure dependence, and along a slab geotherm it decreases by a factor of three at pressures from 14.4 to 18.4 GPa. This rate reduction provides an explanation for the rarity of superdeep diamonds from the interior of the mantle transition zone.

Plain Language Summary

Superdeep diamonds originate from great depths inside Earth, carrying samples from inaccessible mantle to the surface. The reaction between carbonate and iron may be an important mechanism to form diamond through interactions between subducting slabs and surrounding mantle. Interestingly, most superdeep diamonds formed in two narrow zones, at 250-450 km and 600-800 km depths within the ~2700-km-deep mantle. No satisfactory hypothesis explains these preferred depths of diamond formation. We measured the rate of a diamond forming reaction between magnesite and iron. Our data show that high temperature promotes the reaction, while high pressure does the opposite. Particularly, the reaction slows down drastically at about 475($\pm$55) km depth, which may explain the rarity of diamond formation below 450 km depth. The only exception is the second zone at 600-800 km, where carbonate accumulates and warms up due to the stagnation of subducting slabs at the top of lower mantle, providing more reactants and higher temperature for diamond formation. Our study demonstrates that the depth distribution of superdeep diamonds may be controlled by reaction rates.

1 Introduction

Sublithospheric diamonds (superdeep diamonds) compose only ~1% of the total amount of mined diamonds, but they carry unique information on the chemical and thermal states and processes of the Earth's interior (Stachel et al., 2005). While diamond formation is likely ubiquitous at the pressure and temperature conditions of the deep mantle, only a few hundreds of superdeep diamonds have been reported (Harte et al., 1999; Moore & Gurney, 1985; Pearson et al., 2014; Smith et al., 2016; Tappert et al., 2005). Their formation depths, inferred from the compositions of majorite garnet and the aluminum content in bridgmanite inclusions, exhibit an intriguing pattern with very few diamonds from the depth range of 450 to 600 km, corresponding to the interior of the

mantle transition zone (TZ) (Harte, 2010; Stachel et al., 2005). The cause of this gap is unknown.

Superdeep diamonds are related to subducted oceanic slabs because they carry eclogitic inclusions, occasionally with negative Eu anomalies and both ^{13}C depleted and enriched isotopic signatures (Stachel et al., 2000a, 2000b). Redox reactions between carbonates in subducting slabs and metallic iron in the ambient mantle were recently proposed as an important mechanism to produce superdeep diamonds (Rohrbach & Schmidt, 2011). Slab-mantle reactions not only account for carbonate and iron carbide inclusions, reflecting contrasting oxidation states, but also explain abundance patterns of diamond inclusions such as the high frequency and large compositional variability of ferropericlase inclusions (Liu, 2002; Palyanov et al., 2013; Rohrbach & Schmidt, 2011; Walter et al., 2008). This mechanism has been validated by several experimental studies (Bataleva et al., 2015; Martirosyan et al., 2015; Palyanov et al., 2013), but data are scarce at the pressures that correspond to the source depths of most superdeep diamonds (Dorfman et al., 2018; Gao et al., 2017; Rohrbach & Schmidt, 2011) and it is not known if the reaction can occur at slab temperatures. Here we conducted *in-situ* experiments to study the influence of pressure and temperature (*P-T*) on the reaction between magnesite and metallic iron in order to better understand the genesis of superdeep diamonds.

2 Materials and Methods

2.1 Diamond anvil cell (DAC) experiments

Symmetric DACs with 300 µm culets were used to generate high pressure. Sample chambers were formed by indenting 260-µm-thick rhenium gaskets to ~40 µm thickness and then drilling holes of 150-µm diameter at the center. The sample consisted of a 10-µm-thick iron foil (purity 99.85%) embedded between 15-µm-thick compressed slices of $MgCO_3$ powder, which was dried at 120 °C for 4 hrs. The structure and composition of the $MgCO_3$ powder was verified by X-ray diffraction (XRD), Raman, and energy dispersive spectroscopy (EDS) analyses (Figure 1 and Figure S1). The $MgCO_3$ served as a reactant, thermal insulator, and pressure medium. Ruby spheres were placed near the iron foil as a pressure marker during compression (Mao et al., 1967). The pressure of every heated spot was determined directly from the XRD patterns of iron at 300 K before heating (Jephcoat et al., 1986; Mao et al., 1986).

Synchrotron XRD experiments were carried out at beamline 16-ID-B, Advanced Photon Source (APS), using a wavelength of 0.4066 Å and a beam size of 6.8×5.0 µm. High temperature was generated by a double-sided laser heating system with a spot size ~30 µm in diameter. The temperature was measured by fitting the thermal radiation spectra with the grey-body approximation (Text S1) (Meng et al., 2015). Samples were heated from ~1000 K to 1800 K at intervals of 50-100 K. The temperature difference

between two sides was held within 50 K for most points. XRD patterns were collected about every 1-3 min during the heating process, which was stopped when the reaction completed or after 100-160 min because of limited beamtime. The XRD data were processed using Dioptas (Prescher & Prakapenka, 2015) and PDIndexer (Seto et al., 2010) software.

Quenched DAC samples were processed using the FEI Nova NanoLab at Michigan Center for Materials Characterization (MC^2) at the University of Michigan. A wedge shape truncation was opened at the center of the heating spot using a focused ion beam (FIB) and the cross section was analyzed with a Scanning Electron Microscope (SEM).

2.2 Multi-anvil (MA) experiments

Reaction experiments were performed using the 1000-ton multi-anvil apparatus at University of Michigan (Li & Li, 2015). COMPRES 10/5 and 8/3 assemblies were used for 12 GPa and 20 GPa experiments, respectively (Leinenweber et al., 2012). Starting materials consisted of a 10-µm-thick iron foil embedded in $MgCO_3$ powder, which was filled into a gold capsule. The sample was dried at 393 K for 18 hrs to minimize moisture. Recovered products were examined with a Renishaw inVia Raman Microscope. They were then coated with aluminum and analyzed for texture and composition using the JOEL-7800FLV SEM at Electron Microbeam Analysis Laboratory (EMAL) of the University of Michigan.

3 Results and Discussion

DAC experiments were conducted between 12.1 to 40.3 GPa (Table S1). At all pressures the time evolution of XRD patterns confirmed production of elemental carbon and magnesiowüstite at the expense of magnesite and iron, and the formation of iron carbides Fe_3C and Fe_7C_3 as intermediate products (Figure 1, S2 & Text S2). FIB and EDS analyses of the recovered samples (Figure S3) corroborate the phase identification from XRD. Production of diamond and (Mg,Fe)O was further verified by MA experiments on the same sandwiched samples at 12 and 20 GPa, 1523($\pm$50) K (Figure S4, S5 & Table S1). The residual carbide phases observed in DAC experiments were fully converted into elemental carbon at 20 GPa with longer heating time at high temperature. Previous studies also suggested production of elemental carbon in a similar reaction at 51-113 GPa (Dorfman et al., 2018). C+(Mg,Fe)O is therefore more stable than $Fe_3C/Fe_7C_3+MgCO_3$ over the entire mantle pressure range. The residual carbides in the products are due to incomplete reaction instead of stability reversal. Our DAC and MA experiments confirm the two-step reaction between magnesite and iron metal, which first forms carbide and then diamond, as found in previous studies (Dorfman et al., 2018; Palyanov et al., 2013; Rohrbach & Schmidt, 2011).

3.1 *P-T* boundary and rate of magnesite-iron reaction

The reaction between magnesite and iron or iron carbide took place only at sufficiently high temperatures, as indicated by the growth of the reaction product (Mg,Fe)O with time (Figure S6). The initiation temperatures at various pressures define a boundary of the onset of reaction that is nearly linear and crosses 1100 K at 14.4 GPa and 1375 K at 40 GPa (Figure 2). This boundary likely corresponds to the temperatures at which the reaction proceeded at sufficiently high rates to be monitored by XRD within the experimental duration, instead of a thermodynamic stability boundary.
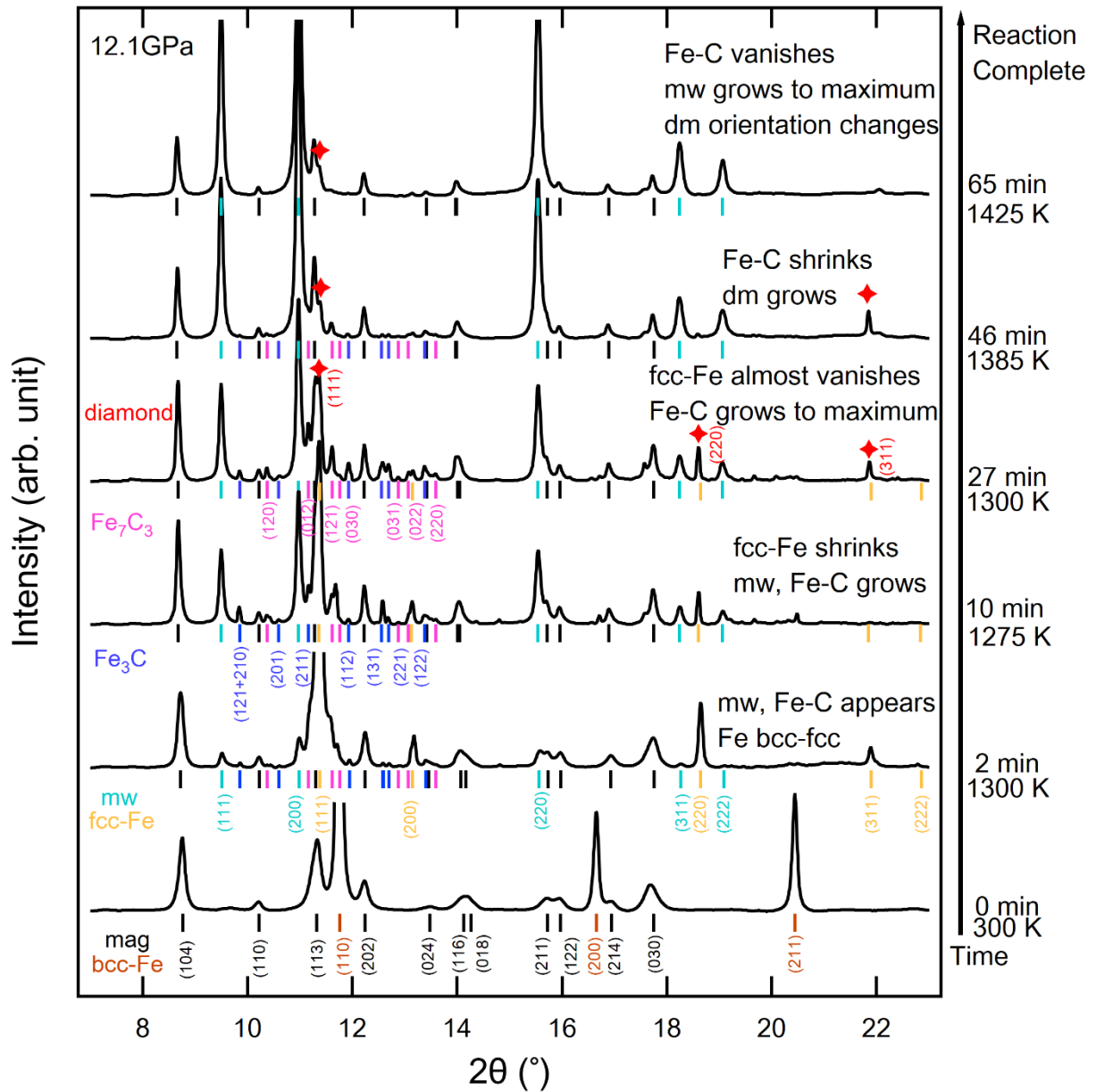
Figure 1. Representative XRD patterns of the iron-magnesite reaction at 12.1 GPa. The starting material consists of magnesite (mag, black) mixed with α-Fe (bcc, brown), which transforms into γ-Fe (fcc, orange) at high temperatures. Iron and magnesite react to produce magnesiowüstite (Mg,Fe)O (mw, cyan) and iron carbides (cohenite Fe_3C, blue and Eckstrom-Adcock carbide Fe_7C_3, magenta). The carbides further react with $MgCO_3$

to form (Mg,Fe)O and diamond (dm, red stars). Strong reflection spots that are consistent with diamond crystals appear after 27 min and persist until the end of the experiment.
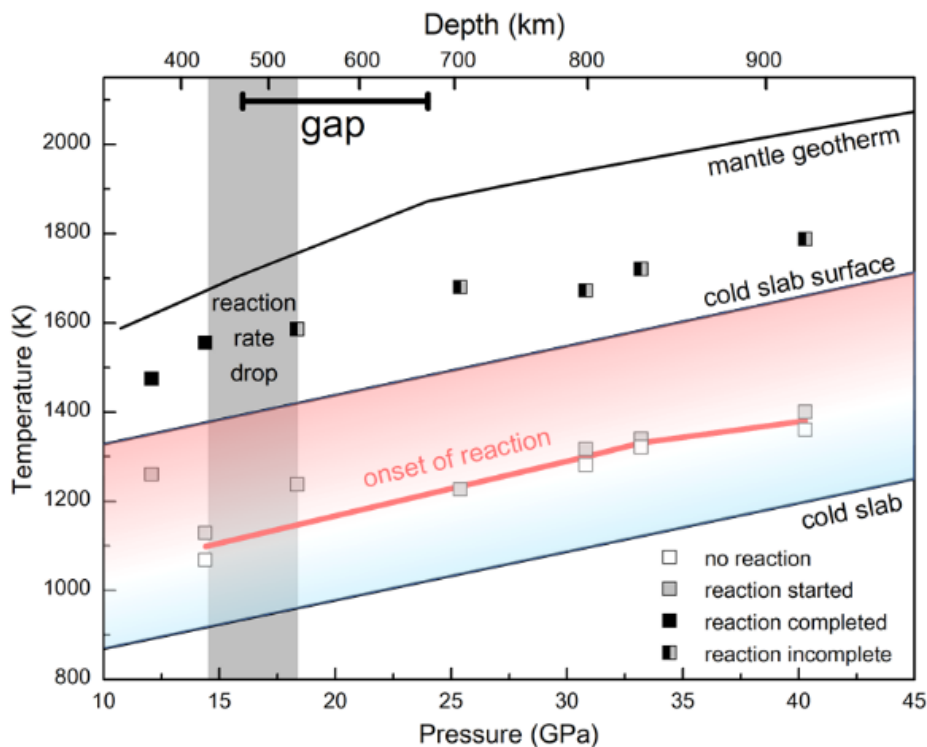

Figure 2. Results of the reaction between iron and magnesite as a function of pressure and temperature. The boundary of the "onset of reaction" (red) is located approximately halfway between the interior and the surface of cold slabs, parallel to the slab geotherm (Brown & Shankland, 1981; Kirby et al., 1996; Syracuse et al., 2010). A drop in the reaction rate occurred between 14.4 and 18.4 GPa (gray zone), which overlaps with the top of a gap in the source depth of superdeep diamonds.

Carbides were exhausted in 1-2 hrs at pressures below 14.4 GPa but persisted to the end of 2-3 hr long heating paths at pressures above 18.4 GPa (Figure 3), indicating a slow-down in the oxidation of carbides within this pressure interval. On a more quantitative level, we estimated the bulk rate of concurrent reactions between magnesite and iron or carbides from the growth curves of the common product (Mg,Fe)O, which formed as fine powder (Figure S7). Barring small variations caused by grain growth and temperature fluctuation, the intensity of (Mg,Fe)O diffraction peaks (111), (200) and

(220) increased at nearly constant rate at a given pressure and temperature (Figure 4a, Figure S8-10), and therefore it appears reasonable to use the growth rate of a (Mg,Fe)O peak as a proxy for the bulk reaction rate.
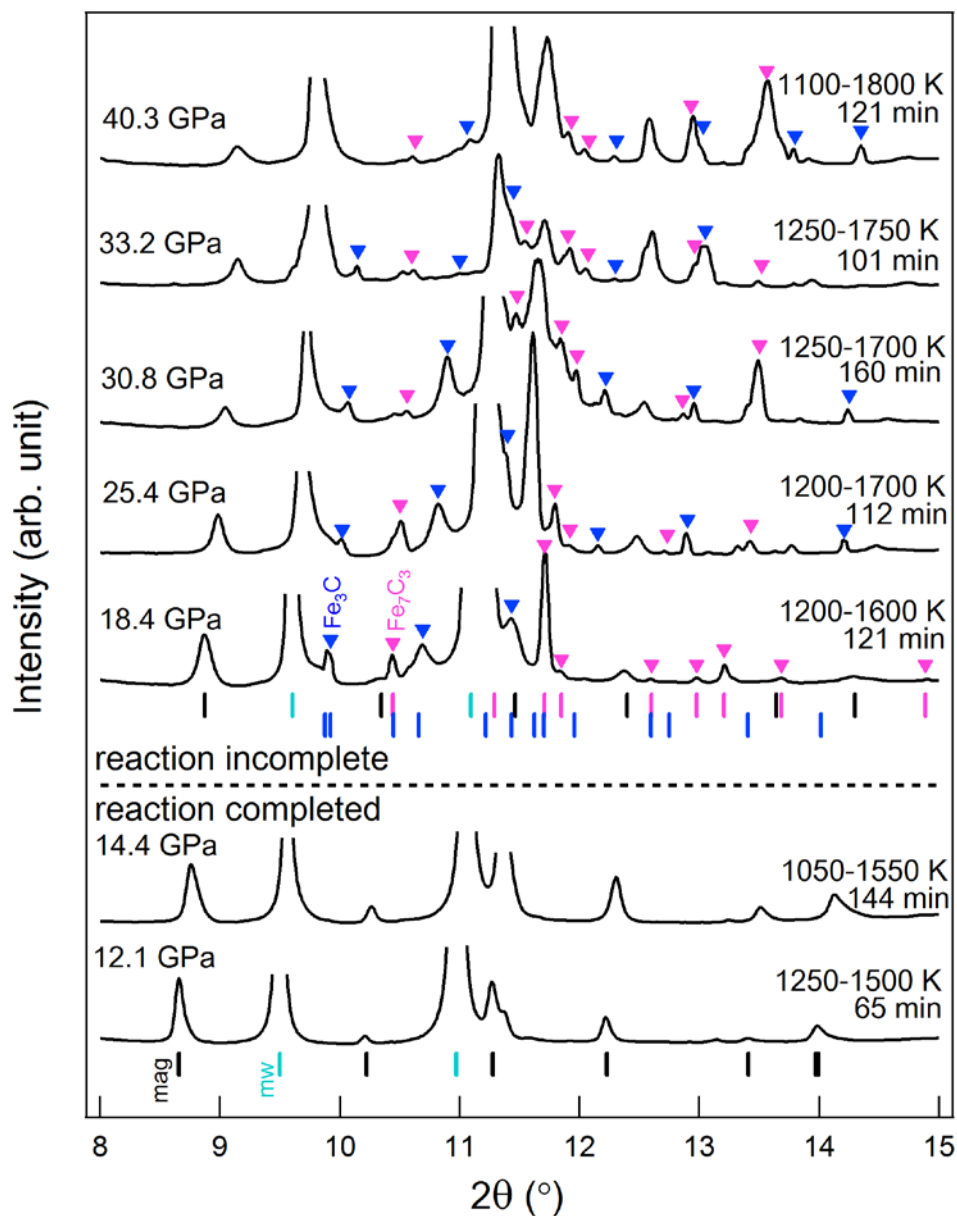

Figure 3. XRD patterns at the end of heating at high pressures. At 12.1 and 14.4 GPa the final patterns contained no iron carbides and only magnesiowüstite (mw, cyan) and excess magnesite (mag, black), indicating complete reaction. At 18.4 GPa to 40.3 GPa

the final patterns contained Fe$_3$C (blue) and Fe$_7$C$_3$ (magenta) together with magnesiowüstite and residual magnesite, indicating incomplete reaction.
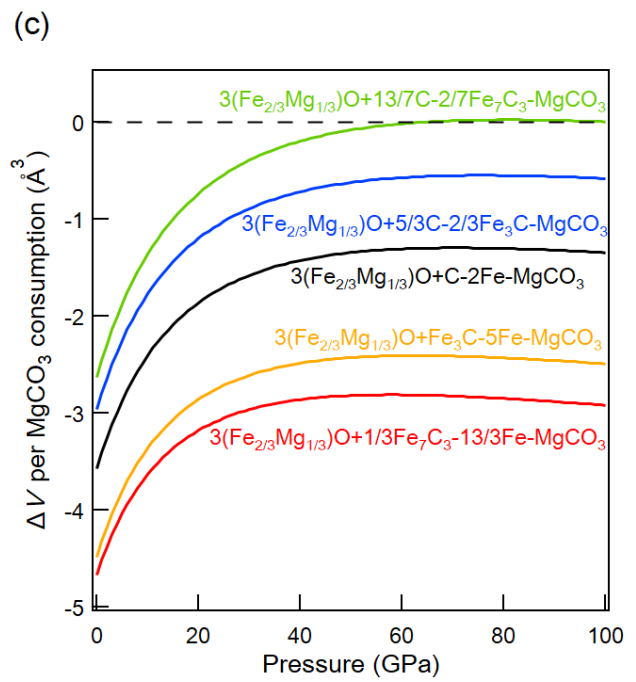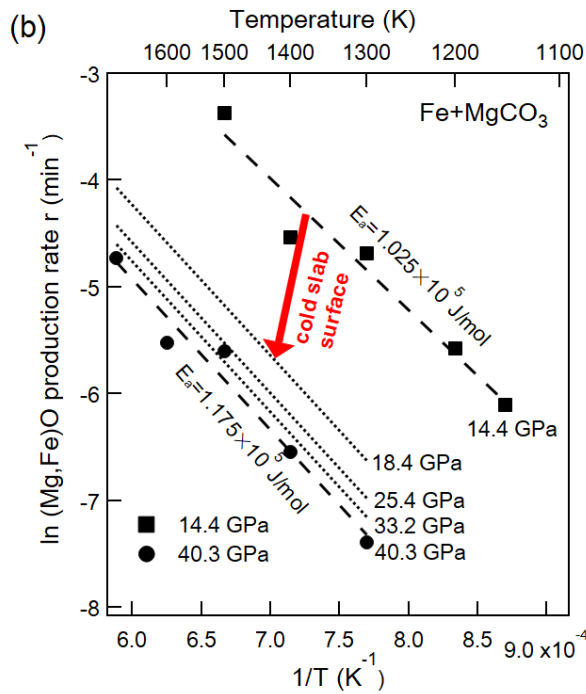
(a)

(b) Fe+MgCO₃

(c)

$E_a = 1.025 \times 10^5$ J/mol

$E_a = 1.175 \times 10^5$ J/mol

cold slab surface

14.4 GPa

18.4 GPa

25.4 GPa

33.2 GPa

40.3 GPa

14.4 GPa

40.3 GPa

$3(Fe_{2/3}Mg_{1/3})O+13/7C-2/7Fe_7C_3-MgCO_3$

$3(Fe_{2/3}Mg_{1/3})O+5/3C-2/3Fe_3C-MgCO_3$

$3(Fe_{2/3}Mg_{1/3})O+C-2Fe-MgCO_3$

$3(Fe_{2/3}Mg_{1/3})O+Fe_3C-5Fe-MgCO_3$

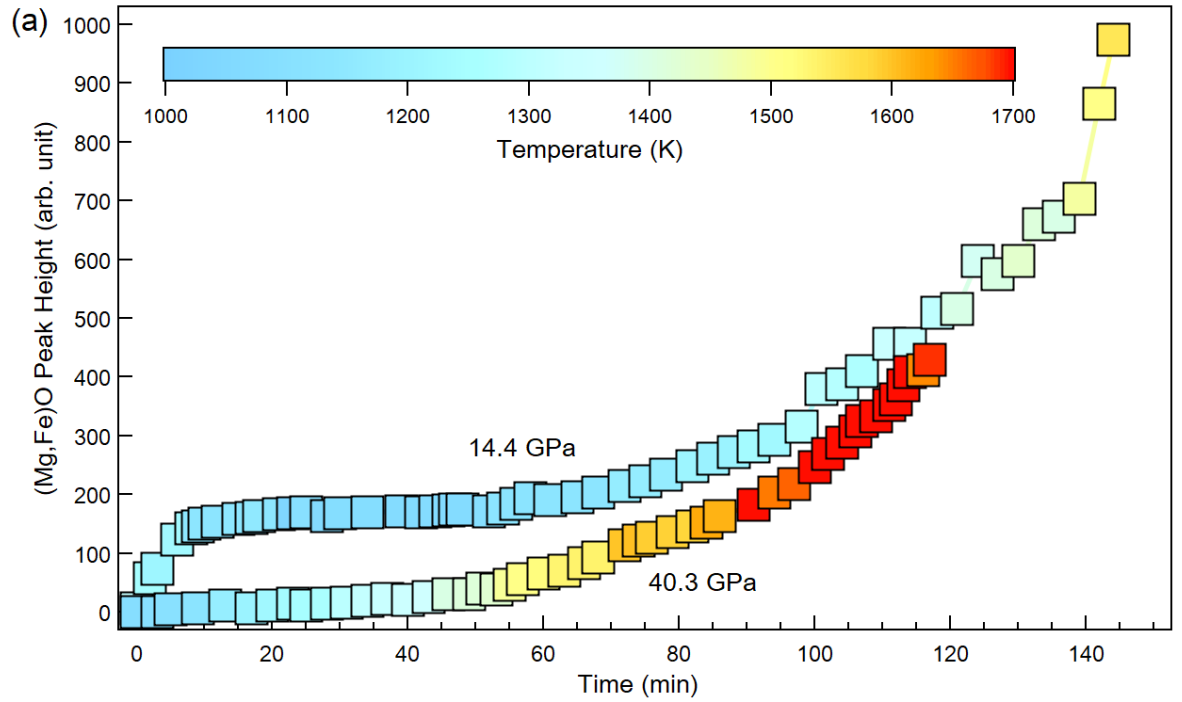$3(Fe_{2/3}Mg_{1/3})O+1/3Fe_7C_3-13/3Fe-MgCO_3$

Figure 4. (a) Height of the (Mg,Fe)O (111) peak as a function of time and temperature. At a given temperature above the reaction boundary, peak height grew continuously with time. (b) Production rate of (Mg,Fe)O *(r)* as a function of pressure and temperature. The production rates of (Mg,Fe)O at 14.4 GPa (squares) and 40.3 GPa (circles) in the same DAC are fitted to an Arrhenius equation (dashed line). The rates at 18.4, 25.4, and 33.2 GPa (dotted lines) from another DAC loading are plotted for comparison (Text S3). Following an estimated geotherm (Kirby et al., 1996), the production rate decreases more than three times between 14.4 GPa-1378 K and 18.4 GPa-1422 K (red arrow). (c) ΔV of all involved reactions as a function of pressure (Text S2) (Dewaele et al., 2008; Fei et al., 2007; Fiquet et al., 2002; Lai et al., 2018; Scott et al., 2001; Tsujino et al., 2013). Dashed line at ΔV=0 indicates equal total volumes between reactants and products. Converting iron to iron carbides (red and orange) has a larger ΔV than converting iron/iron carbides to diamond (black, blue and green). The slope $d\Delta V/dP$ decreases with increasing pressure.

At a given pressure, the reaction rate constant increases with temperature following an Arrhenius-like relationship, which is widely used to describe reaction kinetics at atmospheric pressure (Figure 4b and Text S3). At a given temperature, the reaction rate constant decreases with pressure. Between 14.4 and 18.4 GPa the rate constant drops by a factor of three, leading to the persistence of iron carbides above 18.4 GPa.

The pressure dependence of the rates in solid-state reactions is scarcely studied. In transition-state theory, the rate is related to the activation volume $\Delta V^{\ddagger}$. Considering both forward and reverse reactions, the net rate has a negative dependence on the volume difference between products and reactants, ΔV (Text S3) (Carlson & Rosenfeld, 1981). While $\Delta V^{\ddagger}$ can only be determined empirically and is unknown here, ΔV provides a possible explanation for the observed rate depression with increased pressure (Figure 4c). Over the entire pressure-temperature range studied, the $|\Delta V|$ of oxidizing carbide to produce diamond is smaller than that of oxidizing iron to produce carbide, indicating less driving force to produce diamond than carbide. It coincides with the observation that oxidation of carbides is the rate limiting step (Text S4). Because magnesite has a low bulk modulus and/or diamond has an extremely high bulk modulus, $|\Delta V|$ in all involved reactions decreases rapidly at low pressure when the bulk moduli are low and the relative differences in bulk moduli are high. With increasing pressure, the change in $|\Delta V|$ slows down and occasionally reverses due to the overall increase of bulk modulus and the enhanced effect from the pressure derivative of the bulk modulus. In particular, when the ΔV of converting Fe_7C_3 to diamond approaches zero at high pressure, the transition has little driving force from the volume difference to proceed in either direction. This may explain the persistence of Fe_7C_3 at high pressure as seen here and previously (Dorfman et

al., 2018). The rapid rate reduction at 14.4-18.4 GPa may be partially related to a rapid decrease in ΔV in this pressure range, while the slower rate reduction above 18.4 GPa may be correlated to the slower ΔV depression at higher pressure (Figure 4c). However, $\Delta V^{\ddagger}$ would also change significantly due to the large pressure range discussed here, and this change cannot be theoretically calculated presently. The influence on the pressure dependence of the reaction rate from the $\Delta V^{\ddagger}$ term is still unclear.

The boundary of the onset of reaction follows a similar positive slope as the mantle and slab geotherms and falls half way between the surface and interior of a cold slab (Figure 2), suggesting that the metal-carbonate reaction can take place at the slab-mantle interface to form superdeep diamonds. According to the Arrhenius-like relationship, the reaction rate constant drops rapidly with decreasing temperature (Figure 4b), implying that diamond formation is highly favored near the slab surface over the interior. Because the slab temperatures can vary by more than 200 K through space and time (Richter, 1985; Syracuse et al., 2010), we expect variations in reaction rate at different regions and geological periods.

3.2 Origin of the gap in the depth distribution of superdeep diamonds

Harte (2010) summarized 86 diamonds from 250-450 km depth based on majorite garnet as geobarometer and 251 diamonds from the lower mantle using ferropericlase as a depth indicator (Figure 5a). In 20 diamonds ferropericlase coexists with Ni-free orthopyroxene compositions representing original bridgmanite inclusions, an association that is considered firm evidence for a source region in the lower mantle, and most of them are from the top of the lower mantle at 660-800 km depths, as inferred from their Al content (Harte, 2010; Stachel et al., 2000a; Stachel et al., 2005). Only a handful diamonds with inclusions (three Si-rich majorites with more than 3.4 Si atom per formula unit and one hydrous ringwoodite) come from 450-600 km depths (Harte, 2010; Pearson et al., 2014). The reported hydrous ringwoodite inclusion and many lab experiments demonstrate that wadsleyite and ringwoodite can survive exhumation and therefore the rare occurrence of wadsleyite, ringwoodite and Si-rich majorite may indicate the existence of a "gap" in the depth distribution of diamond formation. A recent study on majorite and Na-majorite inclusions also found that only 12 out of 500 inclusions come from >450 km depths, confirming the upper boundary of the gap in diamond distribution (Beyer & Frost, 2017).

Our experiments suggest that along a slab geotherm (Kirby et al., 1996) the rate constant of the magnesite-iron reaction drops by a factor of three between 14.4 and 18.4 GPa, and then the reaction proceeds at a slower rate at higher pressures (Figure 4b). These results imply a large reduction in diamond production rate at depths greater than

475(±55) km, thus providing a plausible explanation for the rarity of superdeep diamond in the interior of TZ. Near the lower boundary of the TZ, unreacted carbonate may accumulate as a result of slab stagnation at TZ/LM boundary (Fukao et al., 2009; Ringwood, 1982). The increased amount of carbonate at this depth, together with increasing slab temperature during prolonged storage, leads to an increase in production rate with time, which can explain the higher occurrence of superdeep diamonds at 600-800 km depths despite the reduced reaction rate in our experiments.
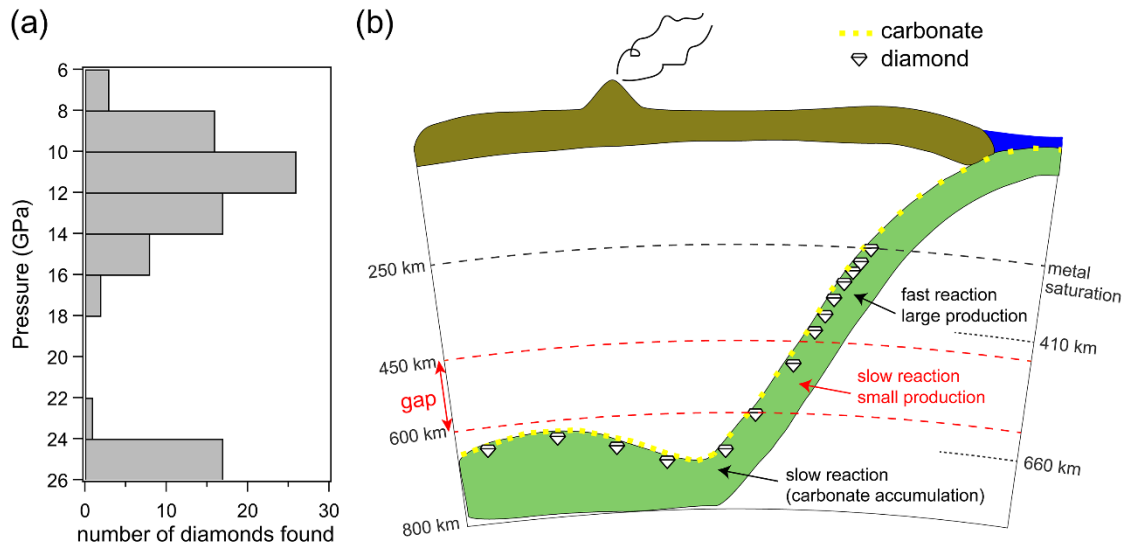
5ure 5. (a) The frequency of diamonds formed at different pressure intervals (Harte, 2010; Pearson et al., 2014), revealing a gap at about 18-22 GPa (~450-600 km). (b) Schematic illustration of diamond production through metal-carbonate reaction at the slab-mantle interface. Diamonds are produced from reaction between carbonates in the subducting slab (yellow dots) and iron metal in the ambient mantle. With continuous replenishment of carbonate from the subducting slab, diamond production in a given period of time is much larger at depth above 450 km, where the reaction rate is higher. As unreacted carbonates accumulate at the site of slab stagnation near the base of TZ, diamond production increases again. All diamonds are assumed to be randomly sampled by plumes, thus their occurrence on Earth's surface in (a) reflects their production in the deep mantle.

3.3 Making diamonds at the slab - mantle interface

In our experiments, carbon formed rapidly from the magnesite-iron reaction at pressures below 14.4 GPa and at a much slower pace at pressures above 18.4 GPa. At all

pressures, however, carbon was produced in just a few hours, so does the rate difference matter in geological processes? The diamond production sites at the interface of the mantle and a subducting slab may be viewed as "factories on a conveyor belt", and our results suggest that the production efficiency of the factories at 250-450 km is at least three times higher than those at 450-600 km depth. If carbonate or metal consumption is not replenished in time, then on a geological time scale the amount of diamonds produced at a given site will depend on the availability of source materials rather than the production efficiency. If, on the other hand, the carbonate and metal consumed are promptly replenished, then the fast "factories" will produce more diamonds than the slow ones in any given period of time, even on a geological time scale.

A subducting slab supplies carbonates continuously at a typical speed of 1-10 cm/year or 1-10 μm/hour . The metal concentration may be maintained through ferrrous iron disproportionation (Rohrbach et al., 2007), driven by metal consumption. Over time, the consumed metal and carbonate near the slab-mantle interface may also be replenished through diffusion, which may occur as fast as 6 cm/year assuming a diffusion coefficient of 10^{-10} m^2/s at 1873 K (Hayden & Watson, 2007). The rate of replenishment is slower than the reaction in our experiments, but may be comparable or faster than the actual rate of diamond production at the slab-mantle interface because the carbonate-metal reaction is limited by low concentrations of the reactants, estimated at ~0.3 wt.% and 0.15-1 wt.% for carbonate and metal, respectively (Dasgupta & Hirschmann, 2010; Frost et al., 2004; Rohrbach et al., 2007). In addition, the rate of reaction between carbonate and metal is likely sensitive to grain size and deformation and may be influenced by the presence of other components. Growth of macro diamond is also slow and requires a specific fluid/melt environment. Further studies are needed to examine these factors and to elucidate the underlying causes of the observed depth distribution.

4 Conclusions and Outlook

In this study, we determined the pressure-temperature boundary of the onset of the reaction between iron and magnesite and relative reaction rates at 12-40 GPa and 1050-1800 K by real-time tracking of XRD peak intensities in laser-heated diamond anvil cell experiments. Our results suggest that diamonds can form through metal-carbonate reaction at the slab-mantle interface. The reaction rate increases with temperature following an Arrhenius-type relationship and decreases with pressure. The reaction rate drops by a factor of three from 14.4 to 18.4 GPa, which may explain the rarity of superdeep diamonds formed below 450 km depth, specifically in the interior of the TZ (450-600 km depth) and in the deep lower mantle (>800 km depth).

Subducting slabs are among the most active regions in the mantle and their interaction with the mantle and core determines the fate of recycled volatiles such as carbon and hydrogen. With continuous replenishment of materials, reactions at the slab-

mantle/core interface are maintained over geological time scales, and the consumption of reactants and accumulation of products depend on reaction kinetics. At present, high-pressure kinetic studies are scarce because it is difficult to observe micro-scale reaction zones and monitor the progress of reactions. By tracking the XRD peaks of reaction products that occur as fine powder, we demonstrated the feasibility of quantifying relative reaction rates to lower mantle pressures and investigating the kinetics of slab-mantle interactions.

Acknowledgments and Data

All data needed to support the conclusions are present in the paper or supplementary materials.

References

Bataleva, Y. V., Palyanov, Y. N., Sokol, A., Borzdov, Y. M., & Bayukov, O. (2015). The role of rocks saturated with metallic iron in the formation of ferric carbonate-silicate melts: experimental modeling under PT-conditions of lithospheric mantle. *Russian Geology and Geophysics, 56*(1), 143-154.

Beyer, C., & Frost, D. J. (2017). The depth of sub-lithospheric diamond formation and the redistribution of carbon in the deep mantle. *Earth and Planetary Science Letters, 461*, 30-39.

Brown, J., & Shankland, T. (1981). Thermodynamic parameters in the Earth as determined from seismic profiles. *Geophysical Journal International, 66*(3), 579-596.

Carlson, W. D., & Rosenfeld, J. L. (1981). Optical determination of topotactic aragonite-calcite growth kinetics: metamorphic implications. *The Journal of geology, 89*(5), 615-638.

Dasgupta, R., & Hirschmann, M. M. (2010). The deep carbon cycle and melting in Earth's interior. *Earth and Planetary Science Letters, 298*(1), 1-13.

Dewaele, A., Datchi, F., Loubeyre, P., & Mezouar, M. (2008). High pressure–high temperature equations of state of neon and diamond. *Physical Review B, 77*(9), 094106.

Dorfman, S. M., Badro, J., Nabiei, F., Prakapenka, V. B., Cantoni, M., & Gillet, P. (2018). Carbonate stability in the reduced lower mantle. *Earth and Planetary Science Letters, 489*, 84-91.

Fei, Y., Zhang, L., Corgne, A., Watson, H., Ricolleau, A., Meng, Y., & Prakapenka, V. (2007). Spin transition and equations of state of (Mg, Fe) O solid solutions. *Geophysical Research Letters, 34*(17).

Fiquet, G., Guyot, F., Kunz, M., Matas, J., Andrault, D., & Hanfland, M. (2002). Structural refinements of magnesite at very high pressure. *American Mineralogist, 87*(8-9), 1261-1265.

Frost, D. J., Liebske, C., Langenhorst, F., McCammon, C. A., Trønnes, R. G., & Rubie, D. C. (2004). Experimental evidence for the existence of iron-rich metal in the Earth's lower mantle. *Nature, 428*(6981), 409-412.

Fukao, Y., Obayashi, M., & Nakakuki, T. (2009). Stagnant slab: a review. *Annual Review of Earth and Planetary Sciences, 37*, 19-46.

Gao, J., Niu, J., Qin, S., & Wu, X. (2017). Ultradeep diamonds originate from deep subducted sedimentary carbonates. *Science China Earth Sciences, 60*(2), 207-217.

Harte, B. (2010). Diamond formation in the deep mantle: the record of mineral inclusions and their distribution in relation to mantle dehydration zones. *Mineralogical Magazine, 74*(2), 189-215.

Harte, B., Harris, J., Hutchison, M., Watt, G., & Wilding, M. (1999). Lower mantle mineral associations in diamonds from Sao Luiz, Brazil. *Mantle Petrology: Field Observations and High Pressure Experimentation: A Tribute to Francis R.(Joe) Boyd, 6*, 125-153.

Hayden, L. A., & Watson, E. B. (2007). A diffusion mechanism for core–mantle interaction. *Nature, 450*(7170), 709-711.

Jephcoat, A. P., Mao, H., & Bell, P. M. (1986). Static compression of iron to 78 GPa with rare gas solids as pressure transmitting media. *Journal of Geophysical Research: Solid Earth, 91*(B5), 4677-4684.

Kirby, S. H., Stein, S., Okal, E. A., & Rubie, D. C. (1996). Metastable mantle phase transformations and deep earthquakes in subducting oceanic lithosphere. *Reviews of Geophysics, 34*(2), 261-306.

Lai, X., Zhu, F., Liu, J., Zhang, D., Hu, Y., Finkelstein, G. J., et al. (2018). The high-pressure anisotropic thermoelastic properties of a potential inner core carbon-bearing phase, Fe_7C_3, by single-crystal X-ray diffraction. *American Mineralogist: Journal of Earth and Planetary Materials, 103*(10), 1568-1574.

Leinenweber, K. D., Tyburczy, J. A., Sharp, T. G., Soignard, E., Diedrich, T., Petuskey, W. B., et al. (2012). Cell assemblies for reproducible multi-anvil experiments (the COMPRES assemblies). *American Mineralogist, 97*(2-3), 353-368.

Li, Z., & Li, J. (2015). Melting curve of NaCl to 20 GPa from electrical measurements of capacitive current. *American Mineralogist, 100*(8-9), 1892-1898.

Liu, L.-g. (2002). An alternative interpretation of lower mantle mineral associations in diamonds. *Contributions to Mineralogy and Petrology, 144*(1), 16-21.

Mao, H., Xu, J.-A., & Bell, P. (1986). Calibration of the ruby pressure gauge to 800 kbar under quasi *hydrostatic conditions. Journal of Geophysical Research: Solid Earth, 91*(B5), 4673-4676.

Mao, H. K., Bassett, W. A., & Takahashi, T. (1967). Effect of pressure on crystal structure and lattice parameters of iron up to 300 kbar. *Journal of Applied Physics, 38*(1), 272-276.

Martirosyan, N. S., Litasov, K. D., Shatskiy, A., & Ohtani, E. (2015). The reactions between iron and magnesite at 6 GPa and 1273–1873 K: Implication to reduction of subducted carbonate in the deep mantle. *Journal of Mineralogical and Petrological Sciences, 110*(2), 49-59.

Meng, Y., Hrubiak, R., Rod, E., Boehler, R., & Shen, G. (2015). New developments in laser-heated diamond anvil cell with in situ synchrotron x-ray diffraction at High Pressure Collaborative Access Team. *Review of Scientific Instruments, 86*(7), 072201.

Moore, R. O., & Gurney, J. J. (1985). Pyroxene solid solution in garnets included in diamond. *Nature, 318*(6046), 553.

Palyanov, Y. N., Bataleva, Y. V., Sokol, A. G., Borzdov, Y. M., Kupriyanov, I. N., Reutsky, V. N., & Sobolev, N. V. (2013). Mantle–slab interaction and redox mechanism of diamond formation. *Proceedings of the National Academy of Sciences, 110*(51), 20408-20413.

Pearson, D., Brenker, F., Nestola, F., McNeill, J., Nasdala, L., Hutchison, M., et al. (2014). Hydrous mantle transition zone indicated by ringwoodite included within diamond. *Nature, 507*(7491), 221-224.

Prescher, C., & Prakapenka, V. B. (2015). DIOPTAS: a program for reduction of two-dimensional X-ray diffraction data and data exploration. *High Pressure Research, 35*(3), 223-230.

Richter, F. M. (1985). Models for the Archean thermal regime. *Earth and Planetary Science Letters, 73*(2), 350-360.

Ringwood, A. E. (1982). Phase transformations and differentiation in subducted lithosphere: implications for mantle dynamics, basalt petrogenesis, and crustal evolution. *The Journal of geology, 90*(6), 611-643.

Rohrbach, A., Ballhaus, C., Golla–Schindler, U., Ulmer, P., Kamenetsky, V. S., & Kuzmin, D. V. (2007). Metal saturation in the upper mantle. *Nature, 449*(7161), 456-458.

Rohrbach, A., & Schmidt, M. W. (2011). Redox freezing and melting in the Earth's deep mantle resulting from carbon-iron redox coupling. *Nature, 472*(7342), 209-212.

Scott, H. P., Williams, Q., & Knittle, E. (2001). Stability and equation of state of Fe_3C to 73 GPa: Implications for carbon in the Earth's core. *Geophysical Research Letters, 28*(9), 1875-1878.

Seto, Y., Nishio-Hamane, D., Nagai, T., & Sata, N. (2010). Development of a software suite on X-ray diffraction experiments. *Review of High Pressure Science and Technology, 20*(3).

Smith, E. M., Shirey, S. B., Nestola, F., Bullock, E. S., Wang, J., Richardson, S. H., & Wang, W. (2016). Large gem diamonds from metallic liquid in Earth's deep mantle. *Science, 354*(6318), 1403-1405.

Stachel, T., Brey, G. P., & Harris, J. W. (2000a). Kankan diamonds (Guinea) I: from the lithosphere down to the transition zone. *Contributions to Mineralogy and Petrology, 140*(1), 1-15.

Stachel, T., Brey, G. P., & Harris, J. W. (2005). Inclusions in sublithospheric diamonds: glimpses of deep Earth. *Elements, 1*(2), 73-78.

Stachel, T., Harris, J. W., Brey, G. P., & Joswig, W. (2000b). Kankan diamonds (Guinea) II: lower mantle inclusion parageneses. *Contributions to Mineralogy and Petrology, 140*(1), 16-27.

Syracuse, E. M., van Keken, P. E., & Abers, G. A. (2010). The global range of subduction zone thermal models. *Physics of the earth and planetary interiors, 183*(1), 73-90.

Tappert, R., Stachel, T., Harris, J. W., Muehlenbachs, K., Ludwig, T., & Brey, G. P. (2005). Diamonds from Jagersfontein (South Africa): messengers from the sublithospheric mantle. *Contributions to Mineralogy and Petrology, 150*(5), 505-522.

Tsujino, N., Nishihara, Y., Nakajima, Y., Takahashi, E., Funakoshi, K.-i., & Higo, Y. (2013). Equation of state of γ-Fe: Reference density for planetary cores. *Earth and Planetary Science Letters, 375*, 244-253.

Walter, M., Bulanova, G., Armstrong, L., Keshav, S., Blundy, J., Gudfinnsson, G., et al. (2008). Primary carbonatite melt from deeply subducted oceanic crust. *Nature, 454*(7204), 622.
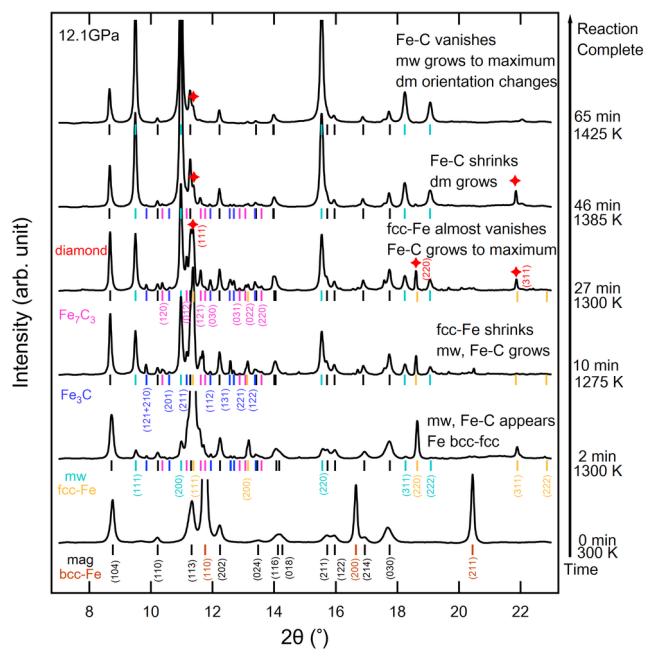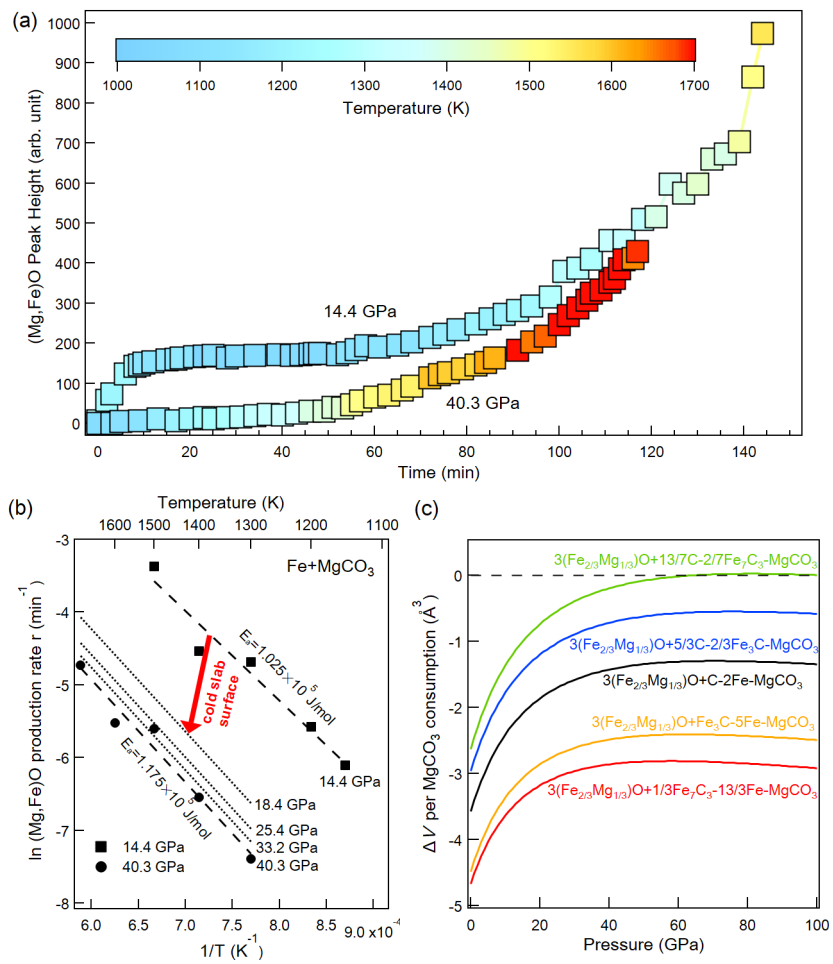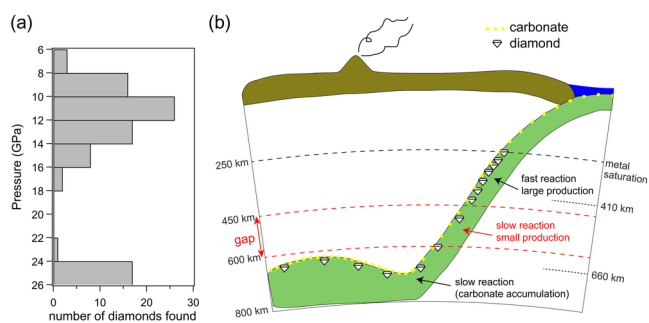
2018GL080740-f01-z-.tif
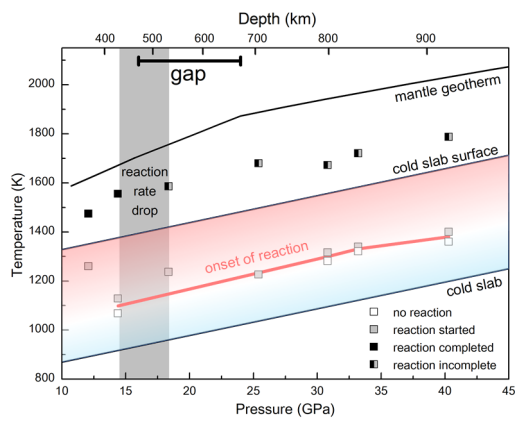
2018GL080740-f02-z-.tif
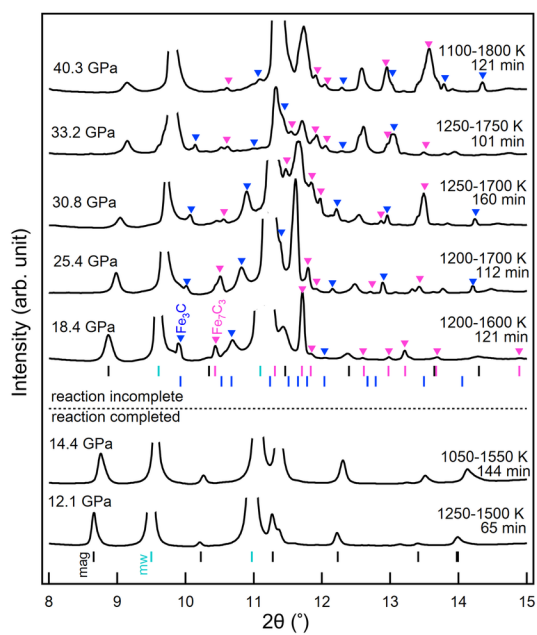
2018GL080740-f03-z-.tif

(a), (b), (c)

2018GL080740-f04-z-.tif

2018GL080740-f05-z-.tif